EFDA–JET–PR(13)47

B. Cannas, A. Fanni, A. Murari, A. Pau, G. Sias
and JET EFDA contributors

Overview of Manifold Learning Techniques for the Investigation of Disruptions on JET

Overview of Manifold Learning Techniques for the Investigation of Disruptions on JET

B. Cannas[1], A. Fanni[1], A. Murari[2], A. Pau[1], G. Sias[1]
and JET EFDA contributors*

JET-EFDA, Culham Science Centre, OX14 3DB, Abingdon, UK

1Electrical and Electronic Engineering Department - University of Cagliari, Italy
2 Consorzio RFX-Associazione EURATOM ENEA per la Fusione, I-35127 Padova, Italy
** See annex of F. Romanelli et al, "Overview of JET Results",*
(24th IAEA Fusion Energy Conference, San Diego, USA (2012)).

Preprint of Paper to be submitted for publication in
Plasma Physics and Controlled Fusion

ABSTRACT.
Identifying a low dimensional embedding of a high dimensional data set allows exploring the data structure. In this paper we tested some existing manifold learning techniques for discovering such embedding within the multidimensional operational space of a nuclear fusion tokamak. Among the manifold learning methods the following approaches have been investigated: linear methods, as Principal Component Analysis, and Grand Tour, and nonlinear methods as Self Organizing Map and its probabilistic variant, the Generative Topographic Mapping. In particular, the last two methods allows us to obtain a low-dimensional (typically 2-D) map of the high-dimensional operational space of the tokamak.

These maps provide a way to visualize the structure of the high dimensional plasma parameters space and allow to discriminate between regions characterized by high risk of disruption and low risk of disruption. The data for this study comes from plasma discharges selected from 2005 and up to 2009 at JET. SOM and GTM provide the most benefits in visualization of very large and high-dimensional datasets. Some measures have been used to evaluate their performance. Special emphasis has been put on the position of outliers and extreme points, quantization errors and topological errors.

INTRODUCTION

One of the most challenging problems in nuclear fusion research consists in the understanding and prediction of disruption events. Disruptions remain indeed the biggest threat to the safe operation of Tokamak devices, and it is crucial to develop proper strategies to avoid/mitigate them. Until now, the comprehension of the disruptive phenomena is far from complete and the literature presents mostly data-driven predictive models. Moreover, it should be noted that there are disruptions of different nature with different temporal scales and, therefore, the final goal of a predictor model is to provide an early enough identification not only of an incoming disruption but also of its specific type.

The identification of the boundaries of the disruption-free plasma parameter space would allow to increase the knowledge on disruptions. However, the analysis and understanding of past experiments require solving the challenges of analyzing massive and complex data sets. Indeed, a huge amount of data is available, due to the large number of experiments and different diagnostics.

A viable approach to better understand disruptive events consists of identifying and explaining the intrinsic structure of the data used to describe the plasma operational space, such as neighborhood relationship, global distribution and clustering. Identifying intrinsic structures is the essence of exploratory data analysis and visualization. Manifold learning algorithms attempt to identify these structures in order to find a low-dimensional representation of the data.

In the present paper, different manifold learning methods have been investigated. Among the linear methods, Principal Component Analysis (PCA) [1], and Grand Tour (GT) [2] have been tested, whereas, among nonlinear methods, Self Organizing Map (SOM) [3] and its probabilistic variant, the Generative Topographic Mapping [4] have been considered.

The available data comes from non-disruptive and disruptive discharges selected from JET

campaigns. In particular, 243 non-intentional disruptions have been considered, that occurred in the JET campaigns from 2005 to 2009 (pulse range 63718 – 79853). Moreover, 1467 safe discharges have been selected, in order to describe also the disruption free operational space of JET.

The paper also proposes some novel measures such as Quantization Error measure, Trustworthiness measure, and Topology Preservation measure, which can be used to provide an objective means by which the mappings can be compared. Until now, it does not appear that these methodologies have been compared in a setting in which the underlying structure of the data may not be known a-priori. Moreover, an outlier analysis has been performed on the available data in order to quantify the goodness of the projection. In fact, in order to preserve the shape of the data cloud, the outliers in the original space have to be projected on the margin of the map.

2. MANIFOLD LEARNING

Finding low-dimensional representations of high-dimensional data is a common problem in science and engineering. It is difficult to display and understand relationships in dimensions higher than two or three. To aid visualization and comprehension of the structure of a dataset, the dimension must be reduced in some way.

Manifold learning is an approach to non-linear dimensionality reduction. Algorithms for this task are based on the idea that the data of interest lies on a low-dimensional manifold, embedded in the high-dimensional space. In mathematical terms, the problem can be stated as follows: given the high-dimensional random variable, find a low dimensional representation of it, that captures the content in the original data according to some criterion.

Data in two or three dimensions can be visualized and the inherent structure of the data and relationships can be better understood. Thus, discovering the best suited manifold would also give the opportunity to form deeper insights into the plasma behavior and the underlying physics.
The manifold learning techniques for dimensionality reduction can be distinguished in linear and nonlinear [5], linear techniques result in each of the components of the new variable being a linear combination of the original variables. In this paper we apply Principal Component Analysis (PCA) [1] and Grand Tour [2]. Such linear techniques are simpler and easier to implement than more recent methods considering non-linear transforms, but often miss important nonlinear structures in the data. For this reason, two nonlinear algorithms have also been applied to map JET operational space, i.e., SOM [3] and GTM [4].

Let us consider the problem of reducing the dimensionality of a given data set consisting of N high-dimensional points in Euclidean space. The high-dimensional input points will be referred to as $\mathbf{T}=\{\mathbf{t}_1,\mathbf{t}_2,....,\mathbf{t}_N\}$ with $\mathbf{t}_i \in \Re^D$. Let L be the dimensionality of the manifold that the input is assumed to lie on. The low-dimensional representations that the dimensionality reduction algorithms find will be referred to as $\mathbf{X}=\{\mathbf{x}_1,\mathbf{x}_2,...., \mathbf{x}_N\}$ with $\mathbf{x}_i \in \Re^L$.

2.1 PRINCIPAL COMPONENT ANALYSIS

PCA finds the L directions (vectors) along which the data has maximum variance and the relative

importance of these directions. If data lies perfectly along an embedding subspace of $\Re^L$, PCA will reveal that subspace; otherwise, PCA will introduce some errors.

Let the first L principal components of $\mathbf{T}$ be $\mathbf{P} = [\mathbf{p}_1,\ldots..,\mathbf{p}_L]$ with $\mathbf{p}_i \in \Re^D$.. The columns of $\mathbf{P}$ are the directions of maximum variation within the data, and they form an orthonormal basis that spans the principal subspace so there is no redundant information.

The data $\mathbf{x}_i$ can be approximated by linear combination of the principal components as $\mathbf{x}_i = \mathbf{P}^T\mathbf{t}_i$, where $\mathbf{P}^T\mathbf{t}_i = \mathbf{c}_i$ are the linear coefficients obtained by projecting the training data onto the principal subspace; that is, $\mathbf{C} = [\mathbf{c}_1,....,\mathbf{c}_N] = \mathbf{P}^T\mathbf{T}$.

Despite PCA's popularity it presents a number of limitations. The main drawback is the requirement that the data lies on a linear subspace. Indeed, when data lies in a low-dimensional manifold, not in a low dimensional subspace, PCA does not correctly extract the low-dimensional structure.

Manifold learning algorithms essentially attempt to duplicate the behavior of PCA, but on nonlinear manifolds instead of linear subspaces.

2.2 GRAND TOUR

The Grand Tour (GT) method, introduced by Asimov [2] and Buja and Asimov [6], is a multivariate visualization method that generates a continuous sequence of low dimensional projections of a high dimensional data set. The animation obtained provides an overview of the high dimensional space in a sequence of 2D plots. Data are looked from all possible viewpoints to get an idea of the overall distribution.

To create a two dimensional Grand Tour, a sequence of planes is generated. The set of planes has to be dense in the data space; the sequence of planes is also required to move continuously from one plane to the next so that the human visual system can smoothly interpolate the data and track individual points and structures in the data. Hence the mathematics of the Asimov-Buja Grand Tour requires a continuous, space-filling path through the set of planes in the high-dimensional data space. Then data has to be projected onto the planes and observed in a time-sequenced set of 2D images.

Several algorithms have been proposed to achieve these two conditions, based on obtaining a general rotation in the high dimensional space.

In this paper the MATLAB implementation in [7] of the Pseudo Grand Tour algorithm, firstly described in Wegman and Shen [8], has been used. The main advantages of the Pseudo Grand Tour, that is an approximate version of the Grand Tour, are speed, ease of calculation, uniformity of the tour, and ease of recovering the projection. However, the algorithm is not space filling, thus only a "pseudo" grand tour is obtained.

2.3 SELF ORGANIZING MAP

A SOM can be intuitively interpreted as some kind of nonlinear PCA. In a SOM the objective is more to preserve the topology, rather than the distance, in the distribution of the data. One natural

way to put this idea in practice consists of replacing the hyper-plane with a discrete (and bounded) grid or lattice defined by some points called prototypes. The prototypes have coordinates in both the embedding and the initial space. They are iteratively fitted inside the data cloud moving the prototypes together with their neighbors in the lattice toward the original data points. Hence, the Self-Organizing Map is a nonlinear dimensionality reduction technique which performs two concurrent subtasks:

- Dimensionality reduction: high dimensional inputs are projected on a low-dimensional regular grid.
- Data clustering and topology preservation: points close to each other in the input space are mapped to the same or neighboring clusters in the output space.

Let us consider in more detail the problem of reducing the dimensionality of a given data set consisting of high-dimensional points in Euclidean space.

The SOM replaces the set of points $\mathbf{T}=\{\mathbf{t}_1,\mathbf{t}_2,.....,\mathbf{t}_N\}$ in the D-dimensional input space $\mathbf{T}$ onto the smaller set of K prototypes points $\mathbf{X}=\{\mathbf{x}_1,\mathbf{x}_2,...,\mathbf{x}_K\}$ with $\mathbf{x}_i \in \Re^L$. Each prototype point in the low-dimensional regular lattice corresponds to a point in the original space. Points close to each other in the input space are mapped on the same or neighboring prototypes in the embedding space. Thus, the SOM simultaneously performs the combination of three concurrent subtasks: vector quantization, dimensionality reduction and topology preservation.

2.4 GENERATIVE TOPOGRAPHIC MAPPING

Generative Topographic Mapping belongs to the class of the so called "generative models", which try in a certain way to model the distribution of the data by defining a density model with low intrinsic dimensionality in the data space.

GTM as a probabilistic counterpart of the SOM, defines a nonlinear mapping from the L-dimensional latent space $\mathbf{X}=\{\mathbf{x}_1,\mathbf{x}_2,.....,\mathbf{x}_K\}$ into the D-dimensional data space $\mathbf{T}=\{\mathbf{t}_1,\mathbf{t}_2,.....,\mathbf{t}_N\}$. The latent space, consists of a regular grid of nodes which is non-linearly projected into data space through Radial Basis Functions (RBF). A Gaussian noise assumption is then made in the data space so that the model becomes a constrained mixture of Gaussians. Thus, each projected point in the data space forms the centre of a Gaussian density function. The model's likelihood is usually maximized by the Expectation Maximization algorithm.

For visualization purposes the latent space is chosen to be 2 or 3-dimensional. The Bayes' theorem is used to invert the transformation from latent to data space allowing to calculate the posterior probability in the latent space for each point $\mathbf{t}$ in the data space.

For visualizing all the data points, it is often convenient to summarize the information provided by the posterior probability distribution and plot its mean or its mode.

GTM can be applied for data clustering and topology preservation. Being the nonlinear mapping described by a smooth function, the topographic ordering of the latent space will be preserved in the data space, in the sense that points close in the latent space will be mapped onto nodes still close in the data space.

With respect to the Self Organizing Map algorithm, GTM defines explicitly a density model (given by the mixture distribution) in the data space, and it allows overcoming several problems, in particular the ones related to the objective function (log likelihood) to be maximized during the training process, and the convergence to a (local) maximum of such an objective function, that is guaranteed by the Expectation Maximization algorithm.

In the following, for easy reading purposes, the clusters in the SOM latent space and the points in the GTM latent space are named *map units*.

3. THE DATA BASE

In this paper, 243 disruptive discharges belonging to campaigns performed at JET from 2005 up to 2009, in the range between Pulse No: 63718 and 79853, have been considered. For each disruptive shot, time of the disruption and disruption class are available [9]. The disruption classes represented in the dataset are Auxiliary power shut-down, Too strong internal transport barrier (ITB), Impurity control problem, Low density and low 'q', Neo-classical tearing mode, Density control problems, Greenwald limit.

The plasma quantities used to describe the plasma operational space are listed in Table I. The choice of these quantities is mainly due to their availability in real-time and their relation to plasma stability. A near identical set of quantities has already been used in literature for disruption prediction and classification purposes [10, 11, 12].

A time instant $t_{pre\text{-}disr}$ has to be defined for the disrupted discharges, which discriminates between the non-disruptive and the disruptive phase. In this paper $t_{pre\text{-}disr}$ has been assumed equal for all the discharges, and it has been set equal to 210 ms, a practical time for JET disruptions. Hence, the dataset for each disruptive pulse consists of the 10 signals made of 210 points each (one sample every 1ms), in the time interval $[t_D - 210 \div t_D]ms$, where t_D is the disruption time.

In the aforementioned shot interval, 1467 safe discharges have been selected, in order to describe also the disruption free operational space of JET.

By analyzing the distributions of the signal values, a proper range of variation for each signal has been assumed to clean the data [11]. Furthermore, for each signal we discarded values within the top and bottom 1%. Being each signal sampled at 1kHz, a huge amount of data is available for describing the safe operational space. Hence, data reduction has been performed on the safe samples belonging to the flat- top phase in order to obtain a balanced data set of safe and disrupted samples [12]. The resulting database is composed of: 222 flat-top disruptions (38900 disruptive samples) and 1467 safe discharges (239965 safe samples).

4. MAPPING OF THE JET OPERATIONAL SPACE

In order to explore the structure of the 10-D JET operational space, graphical methods and manifolds learning algorithms have been applied: Grand Tour, PCA, SOM, and GTM.

As the ranges of variation of the signals are very different, even several orders of magnitude, and since the manifold learning algorithms make use of space metrics, scaling of variables is mandatory.

Hence, before projecting data, each signal in the data base has been normalized by using the min-max normalization.

Further knowledge can be added to the intrinsic knowledge contained in the 10-D data associating a label to each sample in the data set: a safe state is associated with each non-disruptive sample, whereas a disruptive state is associated with each disruptive sample.

4.1 GRAND TOUR

To get an idea of the distribution of the 10-D JET data, a sequence of 2-D images has been generated using Grand Tour algorithm. Figure 1 shows four 2-D scatterplots corresponding to different iterations of the algorithm, i.e. to different viewpoints, where blue points correspond to safe samples whereas red points correspond to disruptive samples. As can be noted, safe regions (blue) and disrupted regions (red) can be identified, even if overlaps are present.

4.2 PRINCIPAL COMPONENT ANALYSIS

In this paper, the resulting principal components have been ordered and the first two (2-D visualization) or three (3-D visualization) components are used as new coordinate axes. In this way, the components that contribute more to the variation in the dataset are retained. The Dimensionality Reduction Toolbox of Matlab [13] has been used.

Figure 2 shows the projection of the JET data onto the first two principal components. Here too, blue points correspond to safe samples whereas red points correspond to disruptive samples. On the left hand side of the figure, the safe points have been plotted before the disruptive ones, conversely on the right hand side the disruptive points have been plotted before the safe ones. As it can be noted, with this representation, two principal components are not enough to clearly separate the disruptive operational space from the safe one.

The 10-D training samples have been also projected on the first three principal components, giving a 3-D visualization of the operational space of JET. Figure 3 reports the 3-D PCA projection. The visualization power of this map is higher than the previous one. However, some overlapping is still present.

Note that PCA performs a linear transformation of the input variables; in order to handle and discover nonlinear relationships between variables, a nonlinear algorithm for dimensionality reduction could be more effective.

4..3 SELF ORGANIZING MAP

The SOM of JET operational space has been presented in [Cannas 2013a]. The map, shown in Figure 4, has 10 input neurons and 4998 map units in the 2-D Kohonen layer. Depending on the map unit composition, four main categories of map units have been distinguished: white empty units, which contain no samples; red disruptive units, which contain disruptive samples; blue safe units, which contain safe samples; gray mixed units, which contain both safe and disruptive samples. The 2-D

SOM in Figure 4 clearly highlights the presence of a large safe region (blue) with an associated low risk of disruption, some disruptive regions (red), with a high risk of disruption well separated from the safe region by transition (grey) and empty regions. Therefore, safe and disruptive states of plasma seem quite well separated in the SOM.

4.4 GENERATIVE TOPOGRAPHIC MAPPING

The GTM of JET operational space has been presented in [12]. In order to compare GTM with SOM, a regular grid of 4900 map units has been considered and the same color code has been adopted (see Figure 5-a).

As the SOM, the GTM presents a large safe region (blue), some disruptive regions (red), well separated from the safe region by transition and empty regions.

Topographic mappings represent a class of dimensionality reduction techniques which try to preserve the underlying structure of the data in the geometric structure of the mapping, making reference to the connection between distances in the high dimensional data space and distances in the projected space onto the map.

The property of distance preservation depends also on the flexibility of the embedding of the lower dimensional manifold in the data space: in other words we have subregions which have to be stretched or shrunk in different way to be properly embedded. Therefore it is important not only the local neighborhood relationships among the different points, usually referred to as topological ordering, but also the neighborhood relations among different subregions of the identified manifold. Regarding the two considered topographic maps of the JET 10-D operational space, it is very interesting to observe how clearly these properties show up by shrinking the SOM along the vertical axis (see Figure 5-b). By comparing the shrunk version of the SOM with the GTM it turns out to be even more evident how much the two identified manifolds look similar. Of course, the different approach in the non-linear mapping gives rise to differences, but to be able to recover so likewise the underlying structure of the data, represents a good starting point that allows us to deal with the obtained mappings with a certain level of confidence.

5. PERFORMANCE ANALYSIS

In order to compare the obtained mappings, some measures can be used to evaluate the performance of each methodology. Special emphasis is put on the position of outliers and extreme points in the maps, and on quantization and topological errors.

5.1 OUTLIERS' ANALYSIS

An outlier is an observation that numerically deviates abnormally from other values of the rest of the population it belongs to. For characterizing abnormal observations there exist different techniques, and, among the graphical ones, scatter plots and box plots are widely employed, revealing outliers' location and distance with respect to the other points of the population.

In the following, the outlier analysis has been used to evaluate the goodness of the mapping. In

fact, the topological shape of the data cloud in the original space is preserved during the mapping if extreme points of the data cloud are mapped to extreme units, located at the borders of the map. The Mahalanobis distance is a measure of statistical distance in a multidimensional space. The points with the greatest Mahalanobis distance are considered outliers. Figure 6 reports the Mahalanobis distance for each point of the dataset with respect to the mean value of the same JET dataset. As it can be seen, the Mahalanobis distances of the safe and disruptive samples are quite different for the two macro-sets.

This is confirmed by using the box plot representation (see Figure 7) of the Mahalanobis distances [14]. On each box, the central mark is the median value, the edges of the box are the 25^{th} (lower quartile) and 75^{th} percentiles (upper quartile), the whiskers extend to the most extreme data points not considered outliers, whereas outliers are plotted individually.

If the lower quartile is Q_1 and the upper quartile is Q_3, then the difference (Q_3 - Q_1) is called the interquartile range or IQR. A data point is usually marked as outlier if it is beyond the following quantity called inner fence:

• Upper/lower inner fence: $Q_3 \pm 1.5 \cdot IQR$

Another more severe condition for identifying outliers takes into consideration a larger threshold on the previous definition that is the outer fence:

• Upper/lower outer fence: $Q_3 \pm 3 \cdot IQR$

A point beyond an outer fence is considered an extreme outlier.

In Figure 7, both for safe and disruptive samples, outliers (marked in red) with respect to inner fences are identified, and, as it can be seen, they are all above the upper one.

In the maps in Figure 8 the green map units contain samples with Mahalanobis distance greater than the upper outer fence. It can be noted that both in the GTM and the SOM, part of the identified outliers are mapped in the borders of the map, whereas the other part is mostly associated with disruptive map units, well separated by transition and empty regions from the safe ones.

Moreover, outliers' location in the learned manifolds is similar for the GTM and the SOM. The difference is emphasized because of the different geometric shape factor of the two maps.

5.2 PERFORMANCE INDEXES

The Average quantization error E_q is a common measure used to calculate the precision of the SOM clustering over the entire dataset [3]:

$$E_q = \frac{1}{N} \sum_{j=1}^{K} \sum_{p=1}^{N_j} \left\| \mathbf{t}_p - \mathbf{b}_j \right\|$$

This error evaluates the fitting of the map to the data and it is determined by averaging the distance of each data vector $\mathbf{t}_p$ from the barycentre $\mathbf{b}_j$ of the N_j data associated to the map unit j to whom $\mathbf{t}_p$ is associated. Thus, the optimal map is expected to yield the smallest average quantization error. Partitions with a good resolution are characterized by low values of E_q.

Literature reports several error indexes to control the conservation of topology, (see [15] and the references therein). Topology preservation has, however, turned out to be quite difficult to define for a discrete grid. In this paper, the "Trustworthiness" of the projected neighborhood and the "Preservation" of the resulting neighborhood have been taken into account.

Trustworthiness measures if data points mapped closed by on the maps are close by in the input space as well [15]. For each data point in the latent space, the set of N_j points belonging to the same map unit constitutes the considered neighborhood. The Trustworthiness of the neighborhood is quantified by measuring how far the data points belonging to the neighborhood in the latent space are from their barycenter in the original space. The distances are measured as rank orders. A measure of the error on the trustworthiness can be expressed as

$$E_{t1} = \frac{1}{K^*} \sum_{j=1}^{K^*} \frac{1}{N_j \left(N - N_j\right)} \sum_{\mathbf{t}_i \in U_{Nj}} \left[rank(\mathbf{t}_i, \mathbf{b_j}) - N_j \right]$$

where K^* is the number of no-empty map units, N_j is the neighborhood size, i.e., the number of samples associated with the j^{th} map unit, $\boldsymbol{b}_\mathbf{j}$ is the barycenter of the N_j vectors in map unit j, $\mathrm{U_{Nj}}$ is the set of the $\mathbf{t}_\mathrm{i}$ vectors associated with the map unit j which are not in the N_j closest to $\boldsymbol{b}_\mathbf{j}$ in the original space, $rank(\mathbf{t}_\mathrm{i}, \boldsymbol{b}_\mathbf{j})$ is the position of vector $\mathbf{t}_\mathrm{i}$ within the sorted list of increasing Euclidean distances from $\boldsymbol{b}_\mathbf{j}$.

A second type of measure analyzes if the original neighborhood is preserved when data are projected. In particular, in the latent space, for the GTM all the points belonging to a certain map unit j will be characterized by the corresponding mode of the posterior probability $\mathrm{mode_j}$, whereas in the case of the SOM they will be characterized by the corresponding prototype vector $\mathbf{x_j}$.
For the GTM the error on the preservation of the original neighborhood can be expressed as

$$E_{t2(GTM)} = \frac{1}{K^*} \sum_{j=1}^{K^*} \frac{1}{N_j \left(N - N_j\right)} \sum_{\mathbf{t}_i \in V_{Nj}} \left[\mathrm{rank}\left(\mathrm{mode}(\mathbf{t}_i), \mathrm{mode_j}\right) - N_j \right]$$

where V_{Nj} is the set of the $\mathbf{t}_\mathrm{i}$ vectors among the N_j closest to $\mathrm{mode_j}$ in the original space which are not associated with the map unit j, and is the position of $\mathrm{mode}(\mathbf{t}_\mathrm{i})$ within the sorted list of increasing Euclidean distances from $\mathrm{mode_j}$.

For Self Organising Maps the corresponding error is

$$E_{t2(SOM)} = \frac{1}{K^*} \sum_{j=1}^{K^*} \frac{1}{N_j \left(N - N_j\right)} \sum_{\mathbf{t}_i \in V_{Nj}} \left[\mathrm{rank}\left(\mathbf{x}\left(\mathbf{t}_i\right), \mathbf{x_j}\right) - N_j \right].$$

where $\mathbf{x}(\mathbf{t}_\mathrm{i})$ is the prototype vector associated with $\mathbf{t_i}$. Note that all the points associated with the same map unit have the same rank.

The quantization errors and the errors on the trustworthiness of the projected data and on the preservation of the original neighborhood are reported in Table II. GTM presents a lower quantization error, i.e., a better fitting of the map to data with respect to SOM. In this case, the map units better represent the data set.

GTM is characterized by a more reliable visualization of the proximities, being the Trustworthiness error one-order lower than SOM. On the contrary, SOM has better performance on the preservation of the original neighborhood. This is not surprising because each dimensionality reduction method necessarily achieves a compromise between the last two kinds of errors.

CONCLUSIONS

This paper aims to test the data visualization capability of some manifold learning algorithms as tools to analyse and understand the high dimensional operational space of a tokamak. Four manifold learning methods have been investigated (Principal Component Analysis, Grand Tour, Self Organizing Maps, and Generative Topographic Mapping) to map the JET high dimensional operational space in lower dimensional spaces. SOM and GTM preserve topology and allow to reveal additional information about the inherent structure of the data, difficult to obtain by the other methods. The results show the superiority of SOM and GTM methods to identify characteristic regions of the plasma scenario, allowing to detect the regions with high risk of disruption, and those with low risk of disruption. These two models provide a non-linear mapping from the observed space to the embedded space.

GTM and SOM have been compared in terms of outliers position, goodness of fitting, trustworthiness and preservation of the neighborhoods.

Outliers' location in the learned manifolds is similar for the GTM and the SOM: some outliers are mapped in the edges of the maps, whereas the others belong to disruptive map units, well separated from the safe ones.

Regarding the precision of the two clustering techniques over the entire dataset, GTM presents a lower quantization error, i.e., a better fitting of the map to data. GTM is also characterized by a more reliable visualization of the proximities. The GTM errors on the trustworthiness of the projected data is one-order lower than in the SOM, whereas the SOM has better performance on the preservation of the original neighborhood. Thus both methods supply important information since each of them achieves a different compromise between those two kinds of errors.

ACKNOWLEDGEMENT

This work was supported by the Euratom Communities under the contract of Association between EURATOM/ENEA. The views and opinions expressed herein do not necessarily reflect those of the European Commission.

REFERENCES

[1]. Jolliffe, I.T. (1986). Principal Component Analysis. Springer-Verlag, **487**.

[2]. Asimov D. (1985). The Grand Tour: a Tool for Viewing Multidimensional Data. SIAM Journal on Scientific and Statistical Computing, **6**(1):128- 143, 1985.

[3]. Kohonen MT (1989) Self-Organization and Associative Memory. Springer-Verlag, New York.

[4]. Bishop, C., Svensén, M., & Williams, C. (1998). GTM: The generative topographic mapping.

Neural Computation, **10**(1), 215–234.

[5]. J. A. Lee, M. Verleysen (2007). Nonlinear Dimensionality Reduction, Springer.

[6]. A. Buja and D. Asimov (1986). Grand Tour Methods: An Outline. In D.M. Allen, editor, Computer Science and Statistics: Proc. of the 17th Symposium on the Interface, pages 63-67, Amsterdam: North Holland, Elsevier Science Publisher B.V.

[7]. Martinez W.L. and Martinez A.R. (2005), Exploratory Data Analysis with Matlab, (London: CRC Press).

[8]. Wegman EJ, Visual data mining (2003) Stat Med. May 15;22(9):1383-97.

[9]. P.C. deVries et al (2011) Survey of Disruption Causes at JET, Nucl. Fusion 51 053018 (12pp).

[10]. Cannas B., Fanni A., P. Sonato, M.K. Zedda, and JET-EFDA contributors (2007) "Real time prediction of disruptions at JET," Nuclear Fusion, vol. **47**, pp. 1559-1569, Nov. 2007.

[11]. Cannas B., Fanni A., Murari A., Pau A., Sias G. and JET EFDA Contributors (2013) Manifold Learning to Interpret JET High-dimensional Operational Space Plasma Physics and Controlled Fusion 55 doi:10.1088/0741-3335/55/4/045006.

[12]. Cannas B., Fanni A., Murari A., Pau A., Sias G. and JET EFDA Contributors (2013) Automatic disruption classification based on manifold learning for real-time applications on JET Nucl. Fusion 53 093023 doi:10.1088/0029-5515/53/9/093023.

[13]. Matlab Toolbox for Dimensionality Reduction v0.7.2 - November 2010.

[14]. Bartkowiak A. Visualizing large data by the SOM and GTM methods — what are we obtaining? (2004) Intelligent Information Processing and Web Mining, Advances in Soft Computing 25, 399-403.

[15]. J. Venna and S. Kaski. Nonlinear dimensionality reduction as information retrieval. In Marina Meila and Xiaotong Shen, editors, Proc. of the 11th International Conference on Artificial Intelligence and Statistics (AISTATS 2007), San Juan, Puerto Rico, March 21-24, pp. 568-575, 2007.

Signals	**Acronym**	**Unit**
Plasma Current	I_p	*A*
Poloidal Beta	β_p	*a.u.*
Mode Lock Amplitude	*LM*	*T*
Safety Factor at 95% of Poloidal Flux	q_{95}	*a.u.*
Total Input Power	P_{tot}	*W*
Plasma Internal Inductance	*li*	*a.u.*
Plasma Centroid Vertical Position	Z_{cc}	*m*
Line Integrated Plasma Density	ne_{lid}	m^{-2}
Stored Diamagnetic Energy Time Derivative	dW_{dia}/dt	*W*
Total Radiated Power	P_{rad}	*W*

Table I: Set of considered signals.

Quality index	GTM	SOM
E_q	0.063	0.155
E_{t1}	0.0011	0.0121
E_{t2}	0.0082	0.0016

Table II: Quantization and topological errors for GTM and SOM

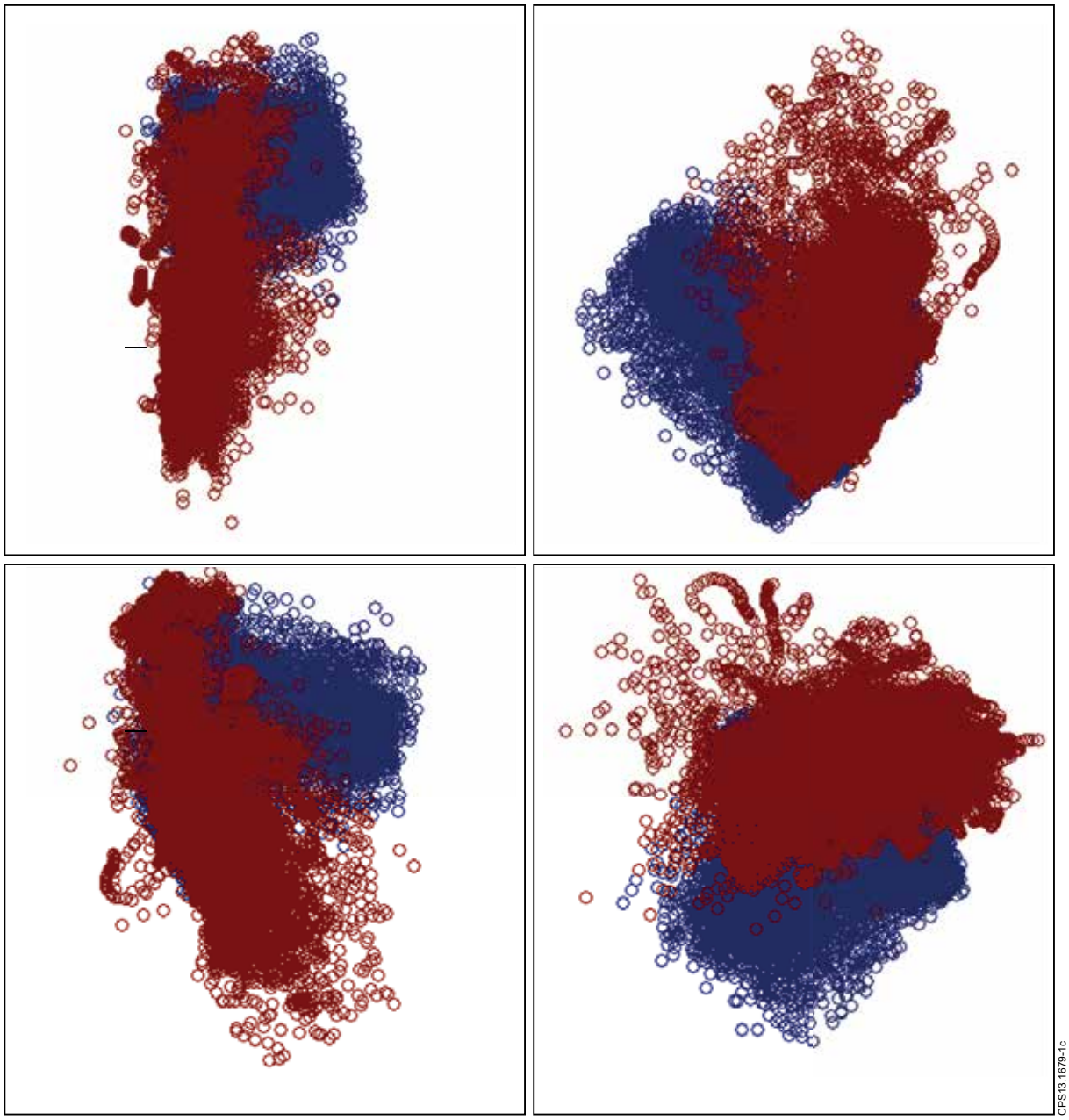

Figure 1: Grand Tour projections of 10-D training disruptive (red) and safe (blue) samples at different iterations.

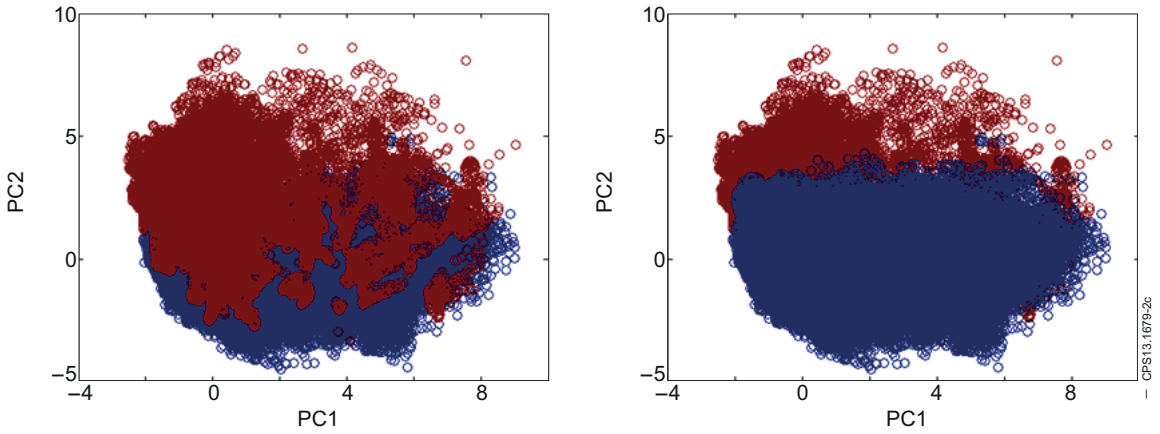

Figure 2: PCA projection of the 10-D training samples on the 2-D PCA; safe samples (blue), disruptive samples (red).

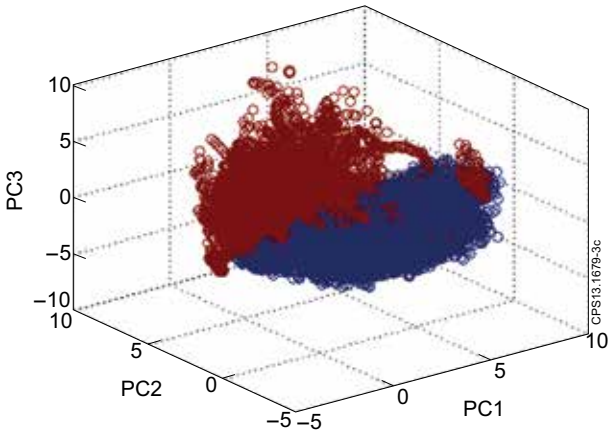

Figure 3: PCA projection of the 10-D training samples on the 3-D PCA; safe samples (blue), disruptive samples (red).

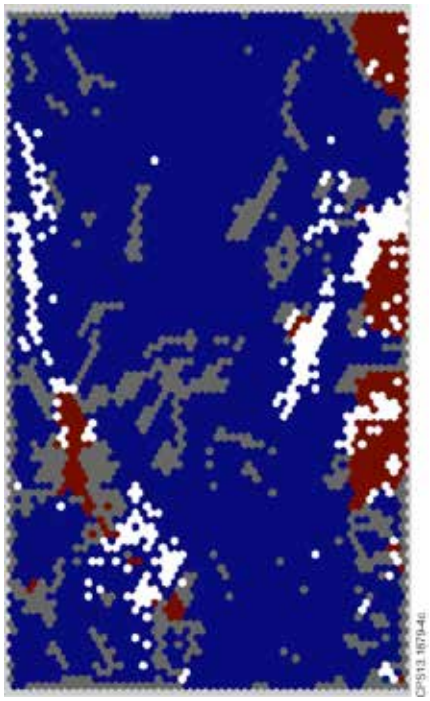

Figure 4: 2-D SOM of the 10-D JET operational space: safe units (blue), disruptive units (red), mixed units (grey), empty units (white).

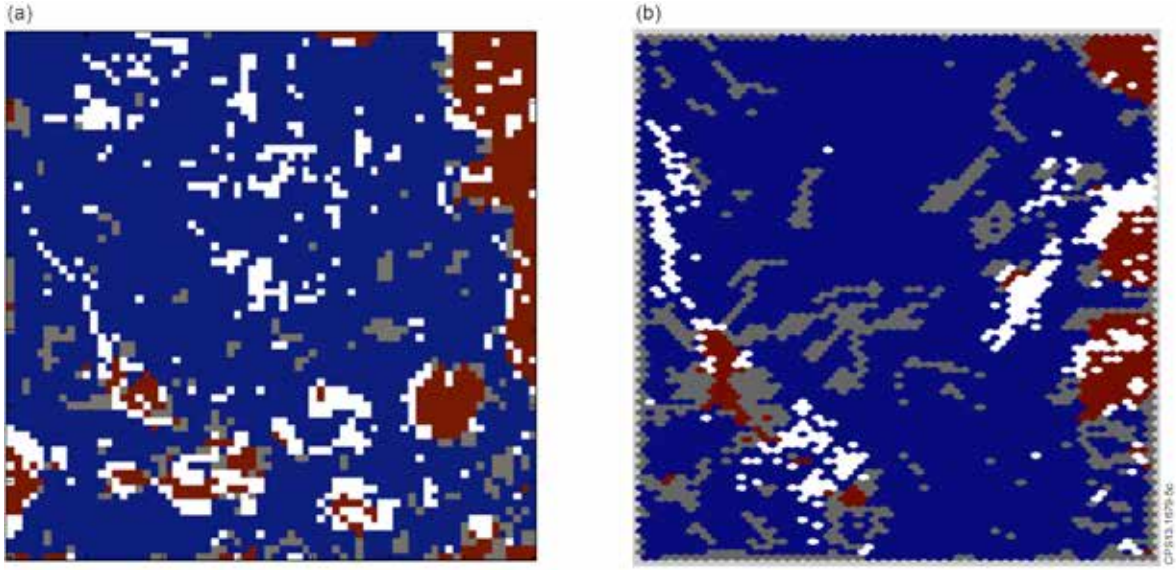

Figure 5: a) GTM of the 10-D JET operational space: safe units (blue), disruptive units (red), mixed units (grey), empty units (white); b) Shrunk version of the SOM in Figure 4.

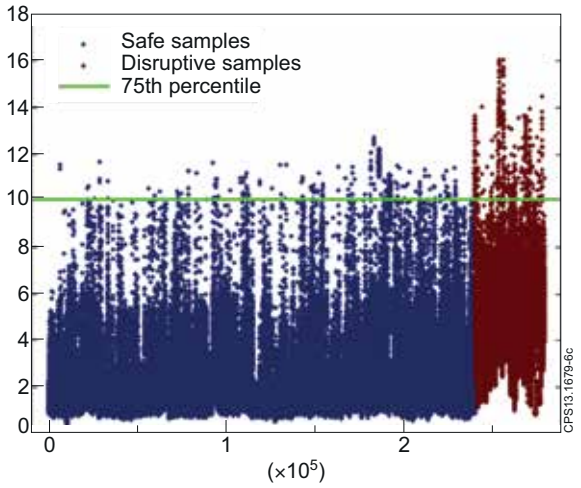

Figure 6: Mahalanobis distance of the safe (blue) and disruptive samples (red) with respect to the mean value of the entire JET dataset.

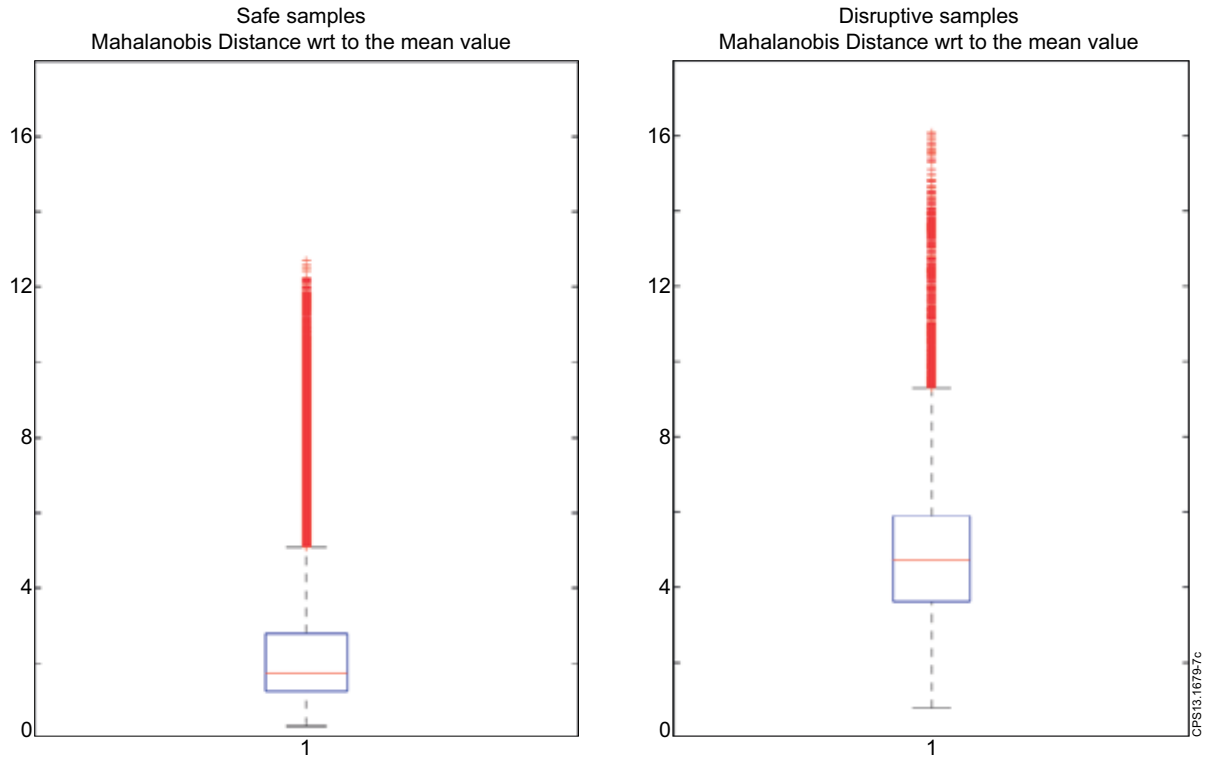

Figure 7: Box plot of the Mahalanobis distance for safe samples (on the left) and disruptive samples (on the right) of JET dataset with outliers marked with respect to the upper outer fence.

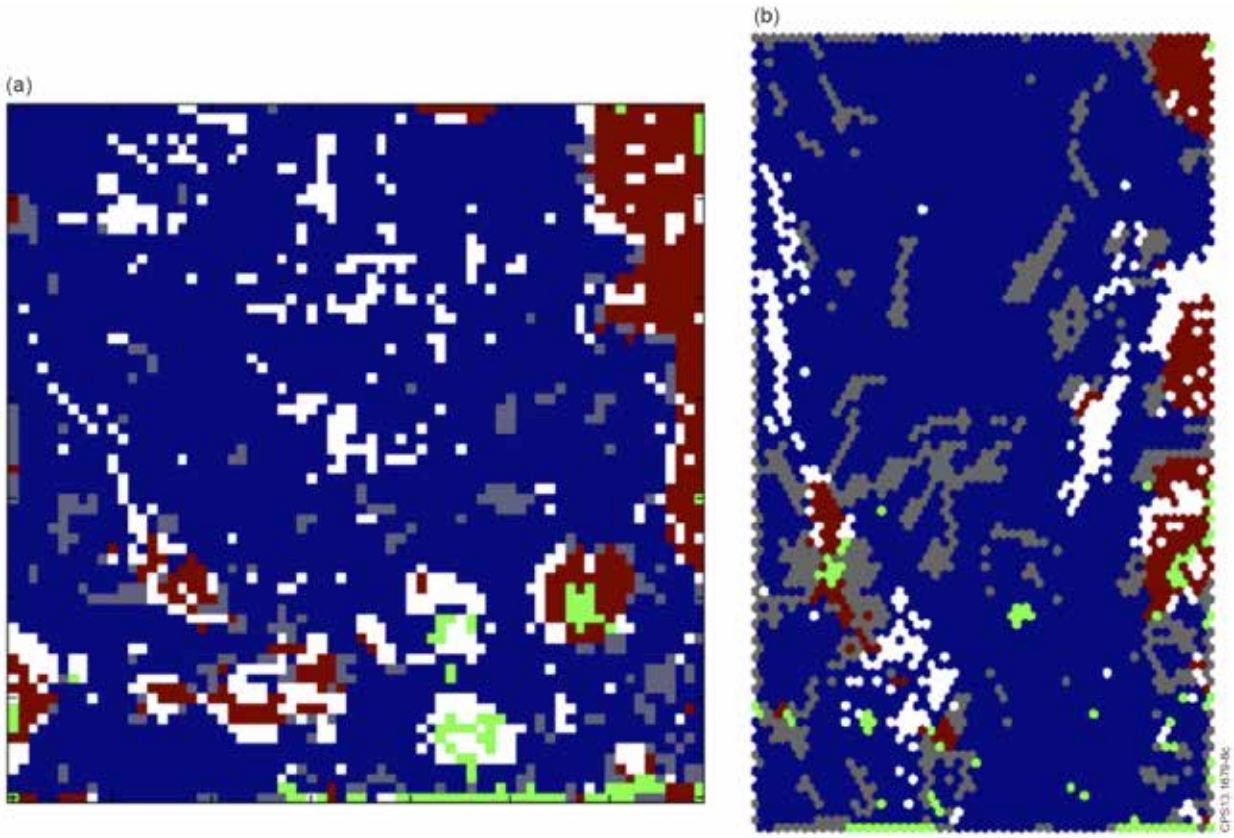

Figure 8: Data points with Mahalanobis distance greater than the upper outer fence (green map units) in the GTM (a) and SOM (b).